ISSN 0252-1075
Research Report No. RR-085

Contributions from
Indian Institute of Tropical Meteorology

NUMERICAL INVESTIGATION ON WIND INDUCED INTERANNUAL VARIABILITY OF THE NORTH INDIAN OCEAN SST

by

S. K. BEHERA,
P. S. SALVEKAR
and
D. W. GANER

PUNE - 411 008
INDIA

APRIL 1999

CONTENTS

Abstract

A 2½ layer thermodynamic numerical ocean model (McCreary et al. 1993, hereafter referred as MKM) is used to simulate interannual variability in the thermodynamic characteristics of the upper Indian Ocean for the period of 1977 to1991. The model is forced by monthly climatology of surface heat flux derived from COADS and the momentum flux derived from interannually - varying monthly mean FSU pseudo stress data. The interannual variability in model simulated fields are thus expected to be in response to changes in wind. The model could simulate the climatological SST very well. Model simulated SST anomalies indicate the positive influence of wind in producing the interannual variability. The time series of SST anomalies in some small regions of Arabian Sea, Bay of Bengal and South-western Indian Ocean are compared with the observed SST anomalies. In general, the phases of the model anomalies are found to be in good agreement with that of observations, but the amplitudes of the model anomalies are under estimated compared to observed anomalies. This suggests that although interannually varying wind can produce the SST variability, but for the realistic extent of such variability, the role of interannual surface heat budget seems to be significant.

The model sensitivity to strong changes in forcing fields is investigated by changing the surface forcing of the first year i.e. 1977. The basin average model SST anomalies show surface cooling (warming) in response to the increased (decreased) wind stress forcing and vice versa in the case of surface thermal forcing. However, the spatial structure of the peak in the anomaly i.e. in July shows warming in most part of the Arabian Sea in the cases of decreased thermal forcing. The strong anomalies thus produced in the first year did not affect the anomalies of the following years.

Key words : Indian Ocean model wind induced interannual SST

1. Introduction

The annual cycle of the monsoon winds induces dramatic changes in the thermodynamic characteristics of the upper north Indian Ocean. The reversal of monsoon winds, the equatorial wave guide and the northern boundaries provide ample mechanisms for the variability in hydrodynamic fields. The local strong southwesterly winds during summer monsoon help in cooling the sea surface by evaporation and upwelling. These local changes in turn excite propagating signals that travel large distances to remotely influence far away regions. For example, these signals that are carried by equatorial Kelvin waves influence the Bay of Bengal circulation. The seasonal variability in the thermodynamic characteristics of the region is understood to some extent but their interannual variabilities are being addressed only recently.

Ocean models provide a reasonable scope for understanding and predicting these fields and their variabilities in both space and time. Uncertainties in estimations and inadequate sampling coverages are some of the reasons that have made model simulation studies so attractive in recent years. Evolution of ocean circulation and heat content in the upper layers generally depend more on the surface forcing fields than on the internal dynamics. Hence, reliable knowledge of the forcings in both space and time is essential for the modelling studies. However, uncertainties still remain in estimating the fluxes, may be due to the sampling problems both in space and time and due to uncertainties in prescribing the drag coefficients, which lead to large discrepancies in different analysis of the fluxes. To avoid sampling problems, climatological fluxes of all the available historical observations for each calendar month are generally used in modelling studies. Therefore, Hellerman and Rosenstein (1983) produced climatological monthly mean wind stress fields over the world ocean are widely used in ocean

modelling studies. Monthly fields of interannual wind stress are also available over some part of the world ocean, e.g. the FSU pseudo-stress fields. However, heat and freshwater flux estimation on any time scale have serious sampling and computational problems. Hence, most of the modelling studies of tropical oceans have been preceded with the observed anomalies only in the momentum flux. Besides their use in the studies of ocean physics and dynamics, ocean models are being coupled with atmosphere models. Atmosphere models also produce momentum fluxes that are more realistic than the other two fluxes.

Since, wind stress is one of the major components of surface forcings in the ocean models, it is crucial to understand model sensitivity to the wind stress forcings. Luther and O'Brien (1989) simulated the interannual variability in the upper layer circulation of the Indian Ocean by forcing a simple reduced gravity model with interannual Cadet and Diehl (1984) wind fields. Although reduced gravity model can not provide many other observed fields, the importance of such simple models can not be ignored due to their simplicity in understanding and interpreting the results. Model studies in the Pacific Ocean suggest a dominating influence of surface wind in determining upper layer thermodynamic structure. The interannual SST variability in equatorial Pacific Ocean is dominantly influenced by the changes in trade winds. However, Pacific Ocean does not experience the large scale seasonal reversal of surface winds and large variability in surface heat flux every year, like monsoon conditions in Indian Ocean. So, in this study a model of intermediate complexity (MKM) is used to examine the contribution of interannual varying surface winds on the SST variability of the Indian Ocean.

2. The Model

The model used in this study is a 2½ layer ocean model fully described in MKM. In short the model ocean has two active layers overlaying a deep motionless layer of infinite depth. The upper two active layers interact with each other through entrainment and detrainment while conserving mass and heat of the total system. In simpler form the surface uppermost layer is a single layer with a thickness of h_1 and temperature T_1 (Fig. 1a). However, once entrainment and detrainment start taking place the surface layer assumes a more complex form in which it separates into two sub-layers i.e. a well-mixed upper turbulent layer of thickness h_m and temperature T_m and a non-turbulent fossil layer of thickness h_f and temperature T_f (Fig. 1b). In both of its simple one layer form and the complex sub-layer form, the surface layer has velocity V_1. Thus, there is no vertical shear in velocity field in the sub-layers of the surface layer.

The uppermost sub-layer of the surface layer that can be termed as upper mixed layer entrains or detrains water in a process in which the mixing is maintained by turbulence generated by both wind stirring and cooling at the surface. The non-turbulent fossil layer i.e. the lower sub-layer of the surface layer being formed by the detrainment of water from the upper mixed layer is kept isolated from the surface turbulence. However, it can be engulfed into the mixed layer either during the strong entrainment periods or upwelling regions where significant decrease of h_1 occurs. There is also provision for detrainment of water from the upper surface layer to the model second layer to conserve mass of the layers as entrainment through the base of the surface layer takes mass from the second layer. In this study the temperature(T_m) of the uppermost turbulent sub-layer is considered as representative of Sea Surface Temperature (SST). The model equations surface forcings are described in the following sub-sections.

2.1 Dynamic equations :

The equations of motion for the upper surface layer are

$$(h_1 V_1)_t + \nabla.(V_1 h\ V_1) + fk \times h_1 V_1 + h_1 < \nabla p_1 >= \tau$$
$$+\upsilon \nabla^2 (h_1 V_1) + V_2 W_e \theta(W_e) + V_1 W_e \theta(-W_e) - \gamma h_1 U_1 i, \qquad (1)$$

and the equation for layer thickness

$$h_{1t} + \nabla.(h_1 V_1) = \kappa_h \nabla^2 h_1 + W_e$$

and for the second layer are

$$(h_2 V_2)_{t+} + \nabla.(V_2 h_2 V) + f k \times h_2 V_2 + h_2 < \nabla p_2 >= \upsilon \nabla^2 (h_2 V_2) \qquad (2)$$
$$- V_2 W_e \theta (W_e) - V_1 W_e \theta (-W_e) - \gamma h_2 U_2 i$$

$$h_{2t} + \nabla.(h_2 V_2) = \kappa_h \nabla^2 h_2 - W_e + W_c$$

Where the total exchange of water (W_e) between the two layers through entrainment (W_k) and detrainment (W_d) is given by

$$W_e = W_d + \delta W_k \theta(W_k)$$

In the above equations, V_i h_i are instantaneuos values of layer velocity and thickness respectively, $< p_i >$ is the depth averaged pressure gradient in a layer and the subscript i = 1, 2 is the layer index. The surface wind stress is τ, the coriolis parameter is $\mathbf{f = 2\Omega sin\varphi}$ and i and k are unit vectors in the zonal and vertical directions. υ, κ_h , κ_T are the coefficients of Laplacian mixing of momentum , layer thickness and temperature. The term W_c is a correction that keeps the total mass in the system fixed to its initial value. The term γ is used to damp U fields at southern open boundary and θ is the heaviside step function, defined as $\theta(x)=1$ if $x > 0$ and $\theta(x)=0$ if $x < 0$. In addition, two symbols, δ and ϕ are defined by $\delta=1$ if $h_f = 0$, $\delta=0$ if $h_f > 0$, and $\phi = 1 - \delta$.

The depth-averaged pressure gradients in each layer are :

$$<p_1> = \alpha g \nabla[h_1 (T_1 - T_d) + h_2 (T_2 - T_d)] - \frac{1}{2}\alpha g h_1 \nabla T_1$$
$$<p_2> = \alpha g \nabla[(T_2 - T_d)(h_1 + h_2)] - \alpha g (h_1 + \frac{1}{2} h_2) \nabla T_2 \qquad (3)$$

where g is the acceleration due to gravity, T_d is the temperature of deep ocean, and

$$T_1 = (h_m T_m + h_f T_f)/h_1$$

is the mean value of T_m and T_f.

2.2 Thermodynamic Equations :

The thickness and temperature of the mixed layer are given by :

$$h_{mt} + \nabla . h_m V_1 = \kappa_h \nabla^2 h_m + \phi W_k + \delta(W_k + W_d) \qquad (4)$$

$$T_{mt} + V_1 . \nabla T_m = \kappa_T \nabla^2 T_m + Q / h_m$$
$$- \phi[W_k \theta(W_k)(T_m - T_f) / h_m] - \delta[W_e \theta(W_e)(T_m - T_e) / h_m]$$

where Q is the heat gain at the ocean surface.

The fossil layer exists only when $h_m < h_1$. The thickness and temperature of the fossil layer are given by :

$$h_f = h_1 - h_m ,$$

$$T_{ft} + V_1 . \nabla T_f = \kappa_T \nabla^2 T_f$$
$$+ W_k \theta(W_k)(T_f - T_m)/h_f - W_e \theta(W_e)(T_f - T_e) / h_f \qquad (5)$$

When $h_m = h_1$, the fossil layer does not exist, and we set $h_f = 0$ and $T_f = T_m$.

The temperature of the fluid entrained at the bottom of the upper layer is T_e and it lies between T_2 and T_m.

The second-layer temperature is given by

$$T_{2t} + V_2 .=T_2 = \kappa_T =^2 T_2 + (T^*_2 - T_2)/t_2$$

$$- W\,\theta(-W_e)(T_f - T_2)/h_2 - W_e\,\theta(W_e)(T_e - T_2)/h_2 \qquad (6)$$

where T^*_2 is the initial temperature of T_2 and t_2 is a time scale.

The model equations are solved numerically on a staggered grid (Arakawa C grid) with T points located at h points and having a horizontal resolution of 55 km over north Indian Ocean (north of 30S). Time integration is done using leap frog scheme with a time step of 1 hour. The fields are averaged between successive time levels at every 41st time step to inhibit time splitting instability.

2.3 Surface forcings

The surface heat flux used as a thermal forcing in the model is derived from the climatological fields of net solar radiation (incoming - outgoing), air temperature, specific humidity and scalar wind magnitudes. These fields were derived from the COADS climatology (Rao et.al.,1991). The data set was prepared at $2^0 \times 2^0$ grid for each month. Linear interpolation is then used in both space and time to get the data at model grid points and at model time steps. For computation of sensible and latent heat fluxes, from these fields bulk formulae with the model predicted SST is used instead of observed climatological SST. The drag coefficient used for computation of these heat fluxes is same as given in MKM.

The wind stress was derived from FSU pseudo stress data (Legler et al., 1989) with drag coefficient $C_D = 1.25 \times 10^{-3}$ and air density $\rho = 1.2$ kg m^{-3}. Bicubic spline interpolation is used to get the data at model grid points. For simplicity model calendar is considered of 360 days having 30 days in each month.

3. Results and Discussion

Initially, the model was spun up for 10 years with Climatological wind stress obtained by 15 year average of FSU winds for the period 1977 to 1991 and Climatological COADS heat flux. The numerical solution reached a quasi-equilibrium state after 9th year. Therefore, the model solutions from 10th year are considered as model climatology for the inter-annual runs in which the model equations are integrated for further 15 years with inter-annually varying mean monthly wind for the period 1977-1991 and with the same climatological heat flux. The values of the model SSTs at 15th day of each month are considered as the representative of the monthly values.

Figure 2. shows the difference between the 15 year averaged (1977-1991) model SST and observed climatological COADS SST for January and July months. In general, the SST difference is noticed to be of the order of $\pm$ 0.5° C in most parts of the basin. This close agreement between model simulation and observed SST is found through out the year, which suggests the model's ability to reproduce seasonal cycle of SST to a reasonably good accuracy. Model SSTs are generally found warmer compared to the observed along the east African Coast, Oman Coast and east coast of India (western boundaries) and are found cooler in the interior oceans. Simplest explanation for such model deficiency might be in the parametrisation of entrainment process which provides stronger representation . in the interior oceans and weaker near coastal regions. However, model results of summer months are closer to the observed one along the Somali Coast indicating realistic entrainments during that season. Model entrains cooler water from lower layer which has got a zonally averaged fixed temperature T_e at its top. In the main run T_e has been derived from climatological SST (MKM). In a sensitivity experiment we derived T_e from the T_2 such that T_2 is assumed to be the value at middle of the second layer and

then extrapolating for T_e to the top of the layer with a climatological basin average constant lapse rate. However, the sensitivity simulation produced similar results as in the main run. Further investigation is being carried out to understand whether these deficiencies are because of the entrainment process or because of the probable errors in surface forcings.

3.1 Interannual variability

Standard deviation (SD) of model SSTs are computed at each grid point to understand the ability of the model in producing SST variability in response to interannual wind. High values of SD are seen in the equatorial region, along African Coast, along west coast of India and southern Indian Ocean (Fig. 3). SD of the order of 0.5° C is seen southwest of India and around 5S, 75E during November (Fig. 3f). These deviations are moving westward and are seen around 5N, 60E and off Somali Coast in January & March respectively (Fig. 3a &b). High variabilities are also seen along Somali Coast (reaching up to 2°C) in May & July (Fig. 3 c & d). Further, to verify whether the variability thus produced is inherent to the model, it was integrated for 15 years with 15 year averaged (1977-1991) wind stress. The SDs thus produced are in general found to be one order less than the previous case, which clearly indicates that the model itself does not produce the interannual variability.

In order to quantify the model performance in producing realistic interannual SST, statistical score like root mean square error (RMS) is computed at each grid point. For this purpose, observed SST analysis of National Center for Environment Prediction (NCEP) is used with a seven month running mean filter to smooth the time series. Since, NCEP SSTs are

available only from 1982, the model SST for the period 1982-1991 is only considered for RMS computation. The RMS error is defined as RMS = $\{\langle(T_m - T_o)^2\rangle\}^{1/2}$, where T_m is the model anomaly, T_o is the observed anomaly for a particular month and $\langle\ \rangle$ represents the ten year average for the considered month. RMS errors are less than 0.5° C in most part of the basin during January (Fig. 4a). However, in July, high values of RMS error are seen near Somali Coast, between 5N & 10N (Fig. 4b). This may be because of model's dependency on surface heat fluxes to produce realistic interannual upwelling patterns. Due to lack of such studies in the Indian Ocean, we could not compare these RMS patterns with other model results to access the performance of the model.

3.2 Variability in individual regions

The time series of the model SST anomalies in three regions viz. (i) southwestern Arabian Sea (55-60E & 5-10N) denoted as AS, (ii) southwestern Bay of Bengal (85-90E & 5-10N) denoted as BB and (iii) southwestern Indian Ocean (55-65E & 15S-25S) denoted as SH(being southern hemispheric region) are shown in figure 5. The observed NCEP SSTs for the three regions during the period 1982-1991 are also shown in the figure for comparison. In general, the phases of model SST anomalies are found to agree with the NCEP SST anomalies. However, the amplitudes of model simulated SST anomalies are much lower than the observed anomalies. This suggests that although the interannual winds could produce the correct phase of SST variability, there is a need for the inclusion of interannual heat flux to simulate realistic amplitude of SST anomalies. The consistent observed colder anomalies during 1984-1986 (Fig. 5.d) are not well simulated in the region AS (Fig. 5a). The observed warm anomaly in 1987 is in good agreement

with model simulation in all the three region. The trend of warming in 1987 can be seen from 1986 in NCEP SST for the region SH which is also simulated by the model. Incidentally, the year 1987 was a bad monsoon year in terms of summer monsoon rainfall for India. Similar trend of warming is also found (with less magnitude) in model simulation before the year 1979, which was also a bad monsoon year. The simulated anomalies are found to be in opposite phase with the corresponding anomalies of wind steering parameter $|\tau|^{3/2}$ (Fig. 6a, b & c). The negative trend of $|\tau|^{3/2}$ anomaly during 1986 may explain the early warming trend in SST in region SH. Negative trend of such amplitude (as seen from seven months running mean line) is not found in any of the three regions during other years. The reason for such trend needs to be investigated in detail which may pose as one of the predictor for Indian monsoon rainfall. The common phenomena of surface cooling in the region AS during summer months is not found in the model simulation for the period 1982-1987 (Fig. 5a), although NCEP SST does show the summer cooling except for the years 1982 ,1983 & 1987. The model behaviour of producing consistent warm phases for the 6 year period is explained by the negative steering parameter values during summer months of those years (Fig. 6a). In region AS, highest warm anomaly of 0.4° C of model SST is found in July 1987 (Fig. 5a). Although a warming of similar amplitude is found in NCEP SST in September 1987, but the highest anomaly of 0.8° C is found during 1983 (Fig. 5d). The less intense model simulation of anomaly in 1983 compared to 1987 is explained by variation in the intensity of the steering parameter (Fig. 6a). Besides AS, similar strong warm anomalies are also found for 1987 in BB and SH (Fig. 5e & f).

Since, AS is dynamically very active region, we further analysed dominant modes of SST variability in the region using empirical orthogonal functions (EOF). Figures 7a - c show the

spatial patterns of the first three dominant modes (which comprises of the 93% of the variability) resulted from the EOF analyses of model simulated anomalies. For comparison we have considered model anomalies only for 1982 - 1991. The corresponding patterns for the three dominant modes of NCEP SST anomalies (comprising of 97% of variability) are shown in Fig. 7d - f . All the three modes of the EOF patterns of model simulated anomalies are quite comparable with that of NCEP SST. The EOF1 that accounts for 73% of the variability in case of model simulation and 88% for the NCEP SST has the same sign all over the region with a core of high at the center. This pattern can be related with the observed recirculation of cold coastal upwelled water around a relatively warm core. Pattern of model EOF2 that accounts for 11% of the variability shows positive sign to the north and negative sign to the south that is comparable to NCEP EOF2 pattern that accounts for 5% of variability. The third EOF mode accounts for 9% of variability in case of model simulation and 4% in case of NCEP SST. The patterns of EOF3 show negative values in the west and positive values in the east which suggest a variability in the upwelled cold water near coastal region. The principle components (PCs) for the corresponding EOFs are shown in figure 8. All the PCs for model simulation show interannual variability and they are in general in phase with the PCs associated with NCEP anomalies. However, amplitude of the model PC1 is lower than that of NCEP anomalies. This also suggests that although interannual variations in winds account for the phase of the maximum SST variability, the interannual changes in heat flux are necessary for producing the realistic amplitudes.

The spatial and temporal variabilities of the summer cooling in the region AS is further analysed by considering latitude - time cross section of SST anomalies along the longitude 55E and north of equator. A seven month running mean is applied to the anomalies to filter the high frequency components. Figure 9 shows the cross section of model simulated SST anomalies for

the period 1977 - 1991 and figure 10 shows the corresponding plot for the NCEP SST anomalies during the period 1982 - 1991. The northward advection of cold anomalies during 1984 and 1985 are found in both observation and model simulations. However, the cold advection in 1986 found in NCEP SST is not well simulated. Model simulation of advection of cold anomalies during 1988 - 1990 are not in good agreement with that of NCEP anomalies but the advection of warm anomalies during 1982, 1983 and 1987 are in agreement.

3.3 Sensitivity experiments

Six sensitivity experiments were carried out to understand the effect of a strong or weak monsoon on the SST of a particular year and the possibility of such anomaly being carried forward to the following years. In all the experiments either surface wind stress or heat flux values or both are increased or decreased all over the basin during the three months period of June - August of the year 1977. The model was integrated for 15 years in each of these cases starting from the model climate (as described in section 3).

In the first experiment, the wind stress values were increased by 1.5 times. Basin averaged SST anomalies obtained from this experiment along with that obtained from main run (section 3.1) are shown in figure 11a. The effect of the increase in the strength of wind stress on SST is evident from the cooling of SST in July. However, the anomaly thus produced did not affect the anomaly of the next succeeding year, i.e. 1978. There is hardly any difference found in the following years between the anomaly produced from this experiment and from that of the main run. The effect of decrease in the strength of wind stress by 0.5 time is shown in figure 11b. The figure shows an increase in the basin averaged peak of 0.4° C in July. As in the previous case,

this warm anomaly also does not affect the anomalies of the succeeding years.

In all the above experiments and in the main run (as described in the previous two sections), climatological surface heat flux values were used as thermal forcing in all the 15 years. In the third sensitivity experiment, this climatic heat flux forcing was increased by 1.5 times during June - August of 1977. The basin average SST anomaly (Fig. 11c) shows a higher warming compared to the previous case. The effect of decrease in heat flux by 0.5 time is shown in Fig. 11d. The cooling produced by the lowering of thermal forcing is almost comparable to the cooling produced by the strong wind case (Fig. 11a). During bad monsoon years, higher positive surface heat flux and lower wind stress are generally observed over north Indian Ocean. In the fifth sensitivity experiment the heat flux was increased by 1.25 times and the wind stress was decreased by 0.25 time to assume a bad monsoon situation. The basin averaged anomalies (Fig. 11e) show an increase in the peak of 0.8° C in July which is less than that found by only increased heat flux case. Note that in the latter case, the heat flux was increased by 1.5 times. In the last experiment, the heat flux was decreased by 0.25 time and the wind stress was increased by 1.25 times to assume a good monsoon year. The basin averaged anomaly in this case (Fig. 11f) shows highest cooling of 0.5° C in July, which is higher than the cooling caused by either increased wind stress or decreased heat flux cases. In all the above experiments, the higher SST anomalies thus simulated during June - August of 1977 are not carried forward to the following years (not even 1978).

Figure 12 shows the corresponding spatial structure of the difference of SST anomalies between main run and the sensitivity experiments in July 1977. In the first case, strong cooling is

inferred near Somali Coast, northern Arabian Sea and Indian coasts (Fig. 12a), that is due to increased entrainment which in turn is caused by stronger wind steering. Most part of the interior ocean and the equatorial region is not affected by the increase in wind stress. In the decreased wind case a similar structure of warming is found with higher intensity along Yemen and Oman coasts (Fig. 12b). Figure 12c shows the spatial structure of SST anomaly in the increased heat flux case. Like previous cases, the warming is higher along the coastal region but in this case, the interior ocean is also affected. In the decreased heat flux case (Fig. 12d), the spatial structure shows both warming and cooling, although the basin average indicates cooling. Pronounced warming is seen along Somali Coast. The strong warming in most part of the Arabian Sea might have resulted by the decrease in the turbulent kinetic energy production, which in turn has reduced the entrainment process. This indicates that the decrease in surface positive heat flux which is normally observed in a good monsoon year, as a result of increased cloudiness, not necessarily will result in cooling of sea surface. Figure 12e shows the effect of increased heat flux and decreased wind. The structure of warm anomaly in this case is similar to that found in the increased heat flux case but has slight reduction in intensity. In the decreased heat flux and increased wind case, the spatial structure (Fig. 12f) of warm anomalies is similar to that of decreased heat flux case. It is interesting to mention that in some experiments, the anomalies created by increasing or decreasing the strength of the wind forcing, even up to 10 times, did not show any effect on the following years. This indicates that the upper mixed layer did ventilate the excess heat with the lower layer. In some other experiments, the strength of forcings was increased or decreased in some particular regions. The SSTs of those regions were found to be most affected and the amplitude of basin averaged anomaly was much reduced.

4. Conclusion

A 2½ layer ocean model (MKM) is used to simulate interannual SST in response to interannual changes in wind stress for the period 1977-1991. The SST climatology computed from the 15 year average of model simulated SSTs is found to be in good agreement with COADS SST climatology. This comparison also suggests that model SSTs are apparently warmer along the African Coast, Oman Coast and east coast of India and are cooler in the interior oceans. These small differences might have resulted because of the over reaction of entrainment process in the interior ocean and less strong entrainment along the western boundaries. In the model, the temperature at the bottom of the first layer from which fluid entrains to top has been derived from zonally averaged climatological SST. The lack of zonal structure in the temperature might have also affected the model SST. However, deriving the entrainment temperature from model second layer temperature did not improve the model SST. The phase of the interannual model SST anomaly is in general, found to be in good agreement with that of NCEP SST anomaly. However, the amplitudes of model anomalies are found to be underestimated. This indicates that the change in wind alone can produce SST variability but the extent of such variability greatly depends on the surface heat budget. The interannual variability in model SST anomalies are found to be in close agreement with that of wind steering parameter. The three individual regions that are considered for closer examination of the variability show the warming trend of 1987. The trend is even noticed towards the end of 1986 in region SH in both model and NCEP anomalies.

The model sensitivity to strong changes in surface forcing is also investigated by changing them in the months of June-August of the first year. The SST anomalies thus produced show warming (cooling) in the corresponding year in response to increased (decreased) wind

stress and vice versa to heat flux. The basin average anomaly shows a peak warming of 1.0° C in case of increased heat flux (1.5 times) and 0.8° C in case of increased heat flux (1.25 times) and decreased wind stress (0.25 time). The peak in cold anomaly produced by increasing the wind stress by 1.5 times is found to be equal to the corresponding anomaly produced by decreasing the heat flux by 0.5 time. However, in the latter case, the spatial structure of SST anomalies also suggests warming in most part of the Arabian Sea. The anomalies thus produced in all the sensitivity experiments are not found to be carried forward to the following years. This suggests that in north Indian Ocean, the strong anomalies produced in any particular year have no effect on the following years.

Acknowledgment : The authors are thankful to the Director, IITM for his interest in the work. They are grateful to Dr. J.P. McCreary for kindly providing the ocean model and helpful suggestions and to Prof J. J. O'Brien and Dr. J. N. Stricherz for kindly providing the wind data. Thanks are due to Dr. Bryan Doty of COLA for kindly providing the GrADS software that was used in the preparation of the figures, to Drs. R.H. Kripalani and M.K. Soman for useful discussions and to Mrs. A.A. Deo for her help during the preparation of the manuscript. This work was carried out on the Silicon Graphics Power Challenge computer of the Institute.

Reference

Cadet, D.L. and Diehl B.C., 1984, "Interannual variability of surface fields over the Indian Ocean during recent decades", Mon.Wea. Rev. 112, 1921-1935.

Hellerman, S. and Rosenstein M, 1983, "Normal monthly wind stress over the world ocean with error estimates", J. Phy.Oceanogr., 13, 1093-1104.

Legler, D.M., Navon J.M, and O'Brien J.J, 1989, "Objective analysis of pseudostress over the Indian Ocean using a direct minimization approach", Mon. Weath. Rev., 117, 709-720.

McCreary, J.P.., Kundu P.K, and Molinari R.L., 1993, "A numerical investigation of dynamics, thermodynamics, and mixed layer processes in the Indian Ocean", Prog. Ocean., 31, 181-244.

Rao, R.R., Molinari R.L, Festa J.F, 1991, "Surface meteorological and near surface oceanographic atlas of the tropical Indian Ocean", NOAA Technical Memorandum, ERLAOML-69.

Reynolds, R.W., Marsico D.C, 1993, "An improved real-time global sea surface temperature analysis.", J. Climate, 6, 114-119.

Luther, M.E. and O'Brien J.J, 1989, " Modelling the variability in the Somali current", Mesoscale/Synoptic coherent structures in Geophysical Turbulence, Eds J.C.J.Nihoul and B.M.Jamart, Elsevier Science Publ. Amsterdam, 373-386.

Figure - 1

(a)

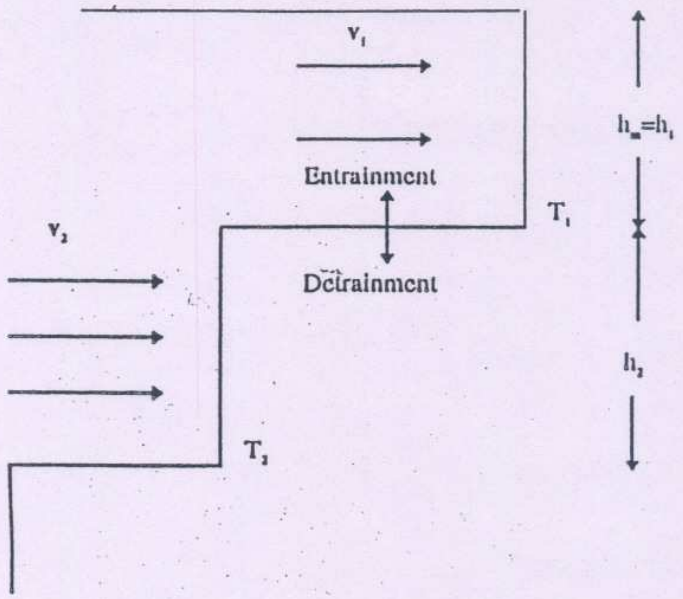

(b)

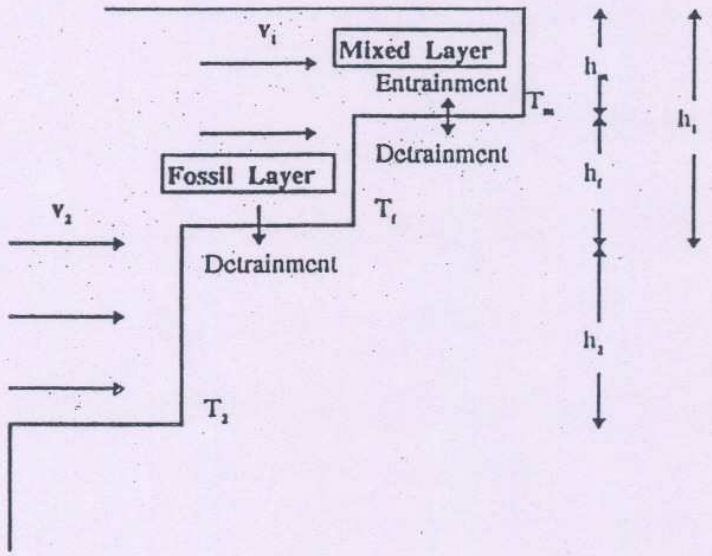

Fig. 1. A schematic diagram of the model layer structure, a) in the simpler form with single upper layer and b) in more complex form when upper layer is divided in to uppermost mixed sub-layer and a second fossil sub-layer.

Figure – 2

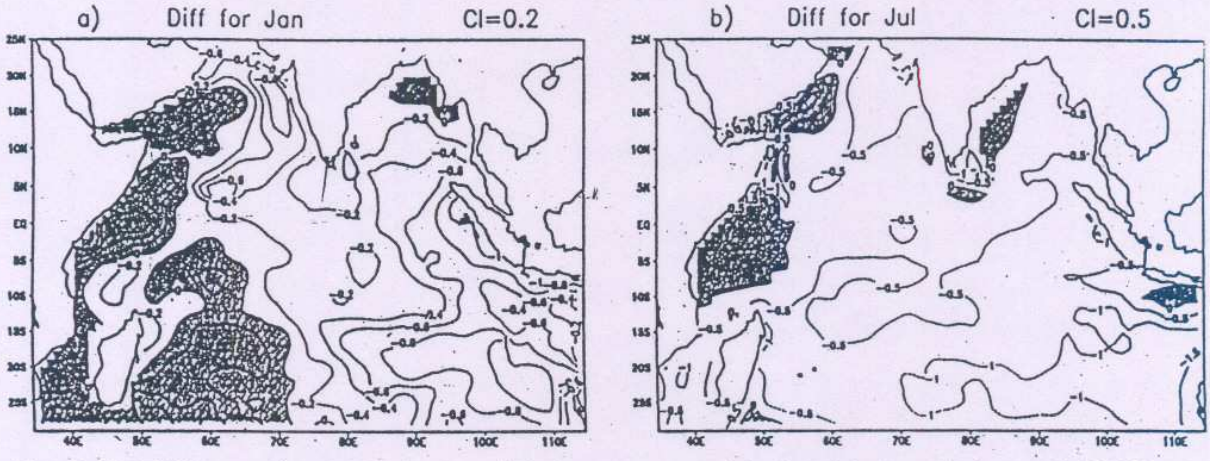

Fig. 2 SST difference (model – observed) between model climatology and observed COADS climatology, a)January and b)July. Positive values are shaded.

Figure - 3

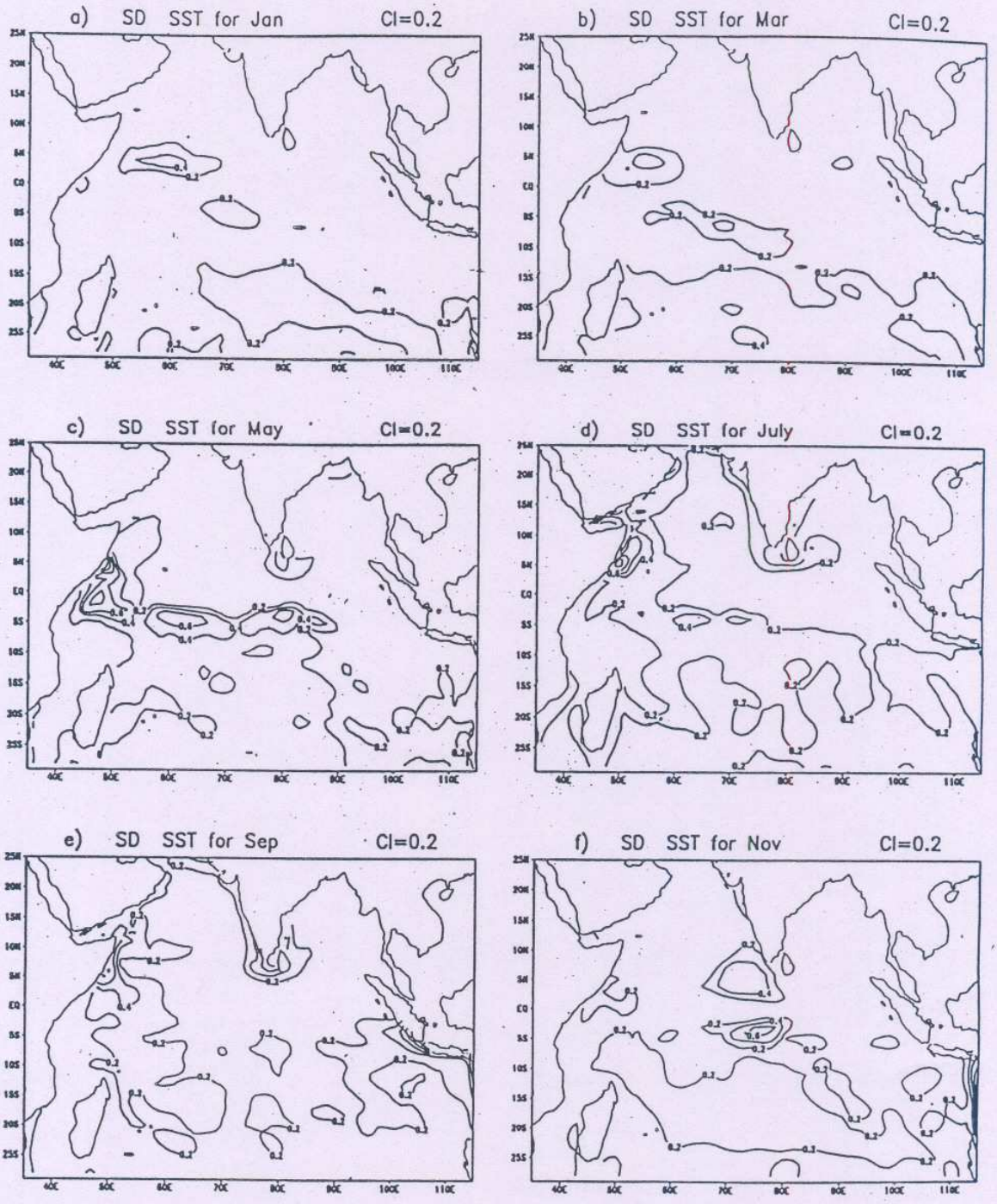

Fig. 3 Standard deviation of model SST fields; a)January,b)March,c)May,d)July,e)September,f)November.

Figure – 4

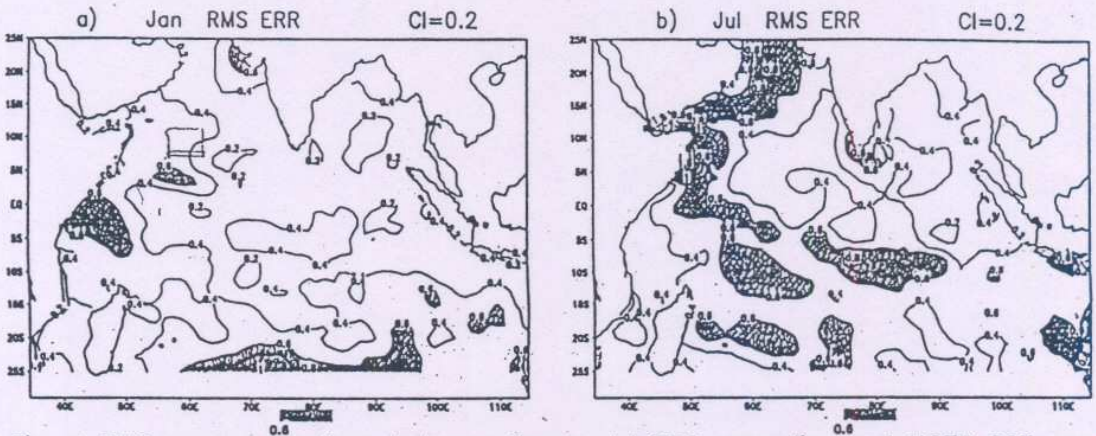

Fig. 4 RMS error evaluation between the model SST anomalies and NCEP SST anom a) January b) July. Values >0.6 are shaded.

Figure -5

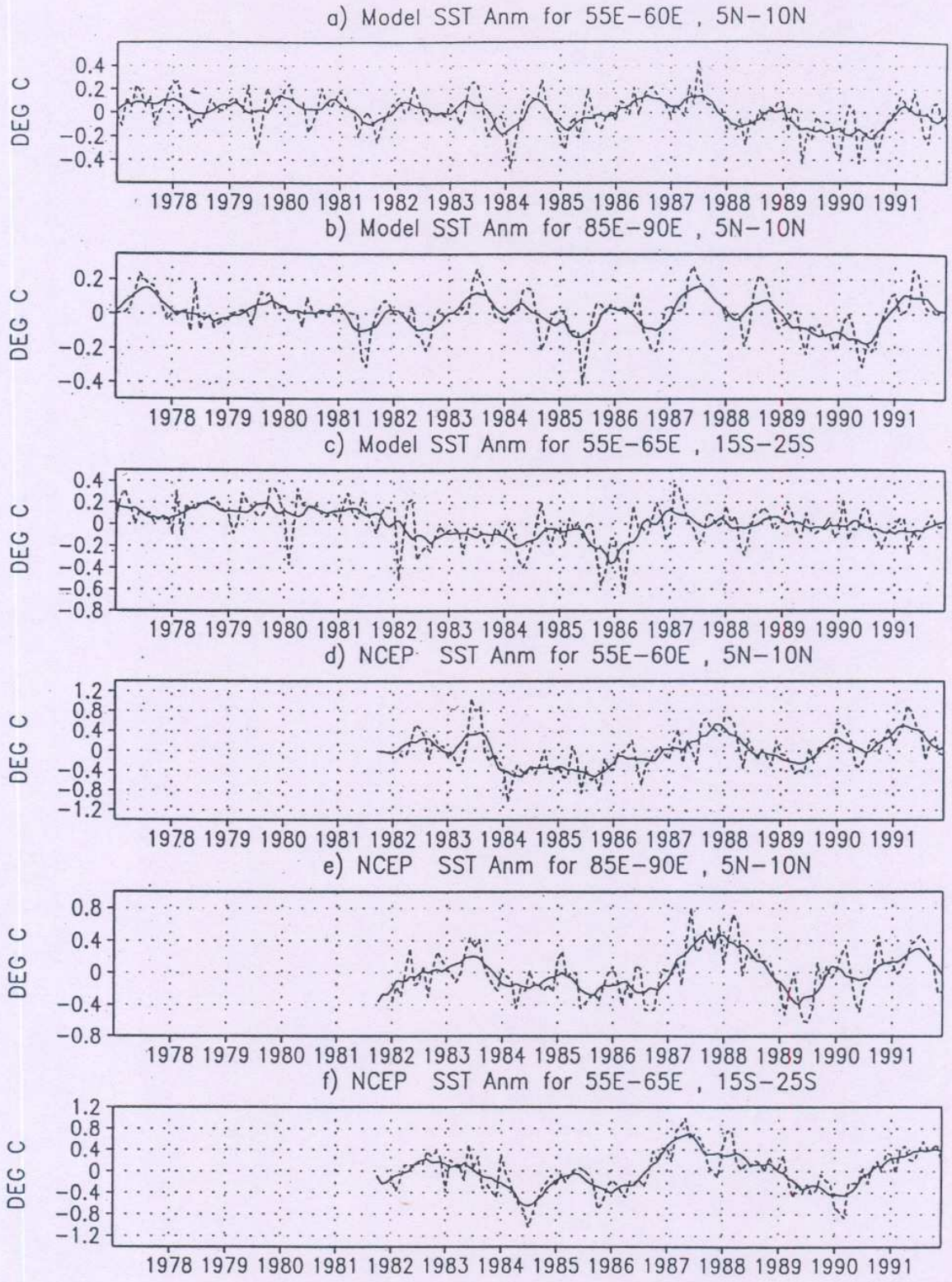

Fig. 5. Time series of SST anomalies (dashed lines) from the ocean model for regions, a) AS, b) BB, c) SH and from observations for regions d) AS, e) BB and f) SH. Superimposed is a 7 month running mean (solid lines).

Figure -6

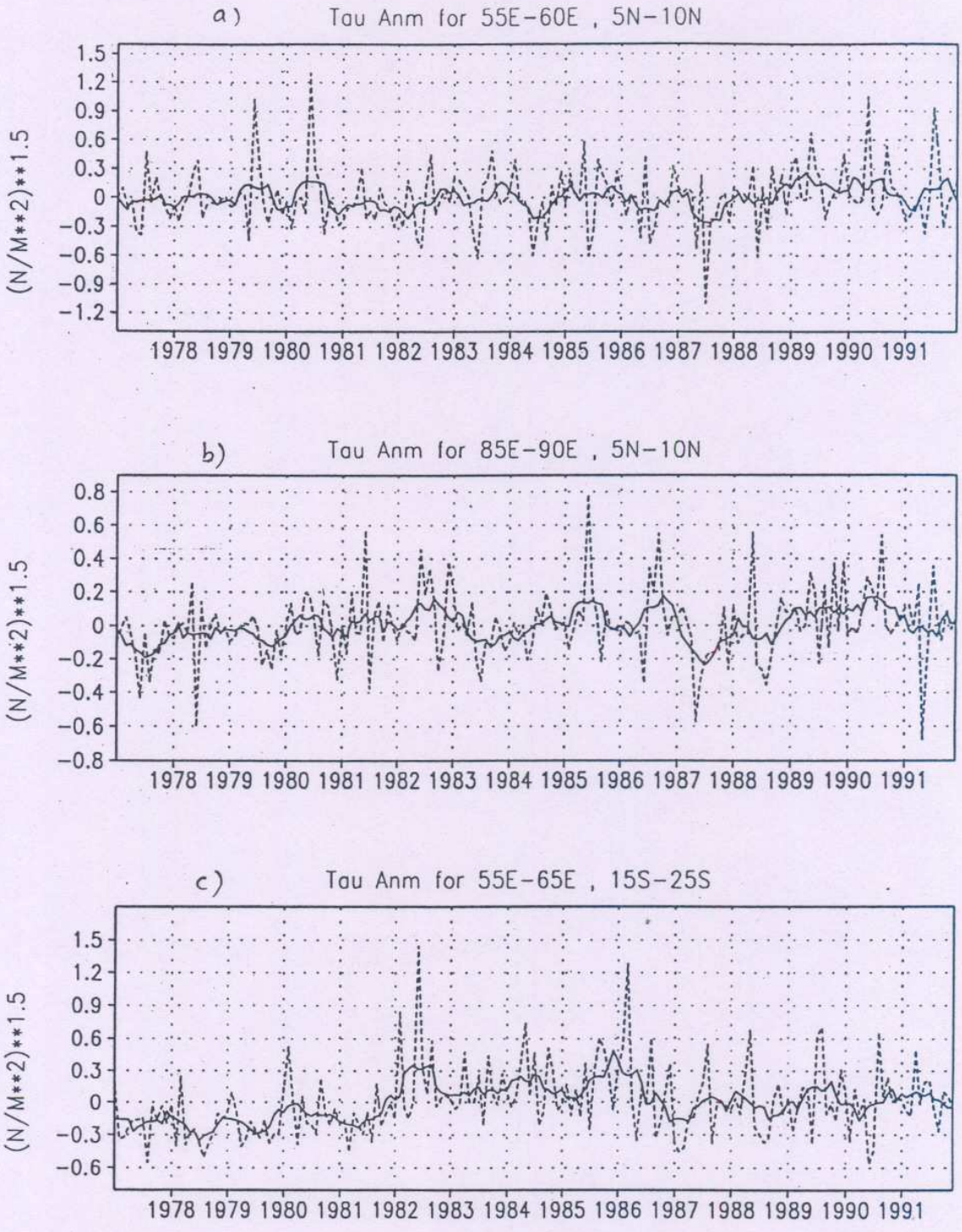

Fig. 6 Time series of the anomaly in wind steering parameter for region a) AS, b) BB and c) SH. Superimposed is a seven month running mean

Figure – 7

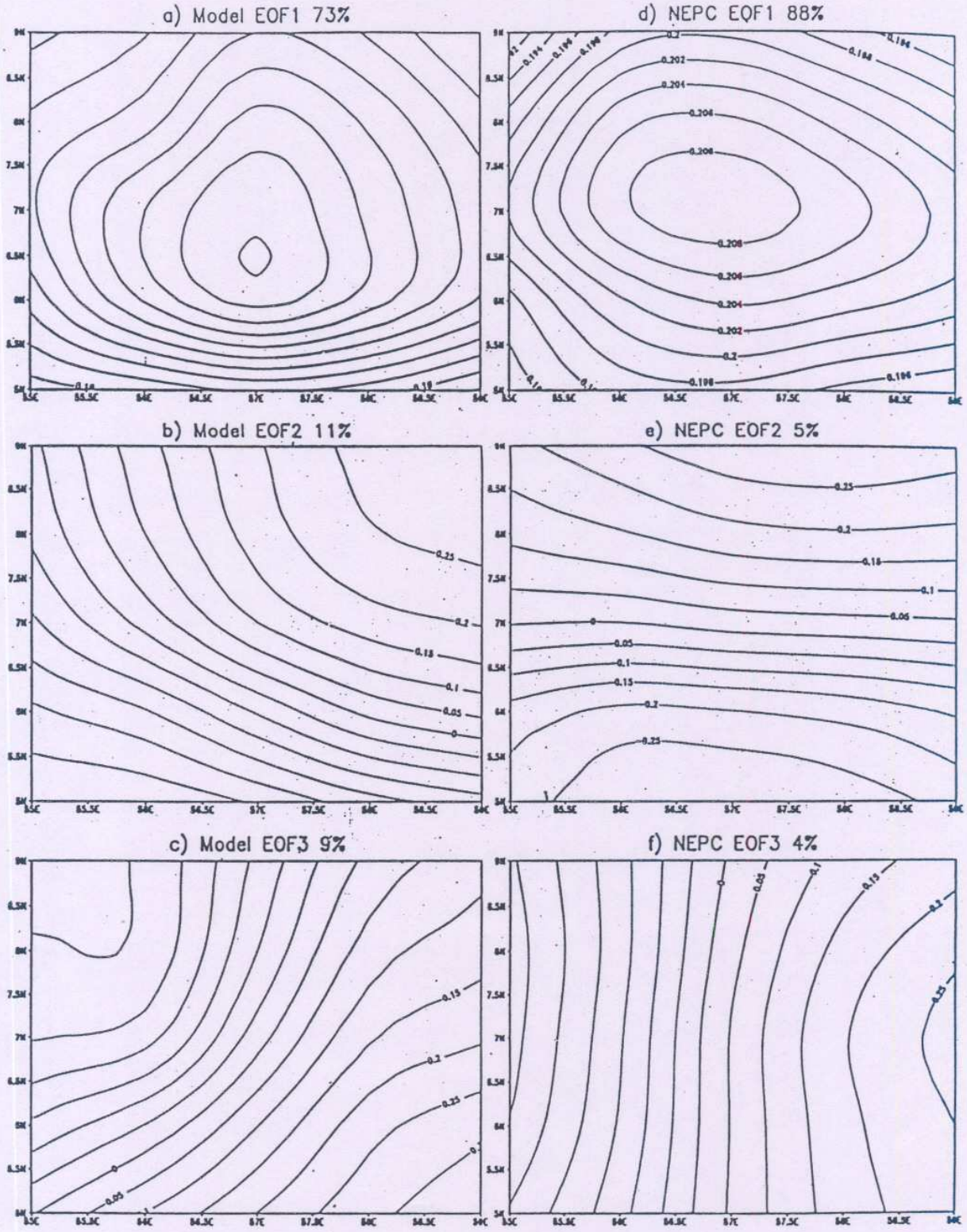

Fig. 7 Empirical orthogonal functions of the model SST anomalies for the period 1982-1991 in region AS, a) EOF1 that accounts for 73% of the total variance, b) EOF2 , 11%, c) EOF3, 9% and for corresponding NCEP SST anomalies, d) EOF1, 88%, e) EOF2, 5%, f) EOF3, 4%.

Figure – 8

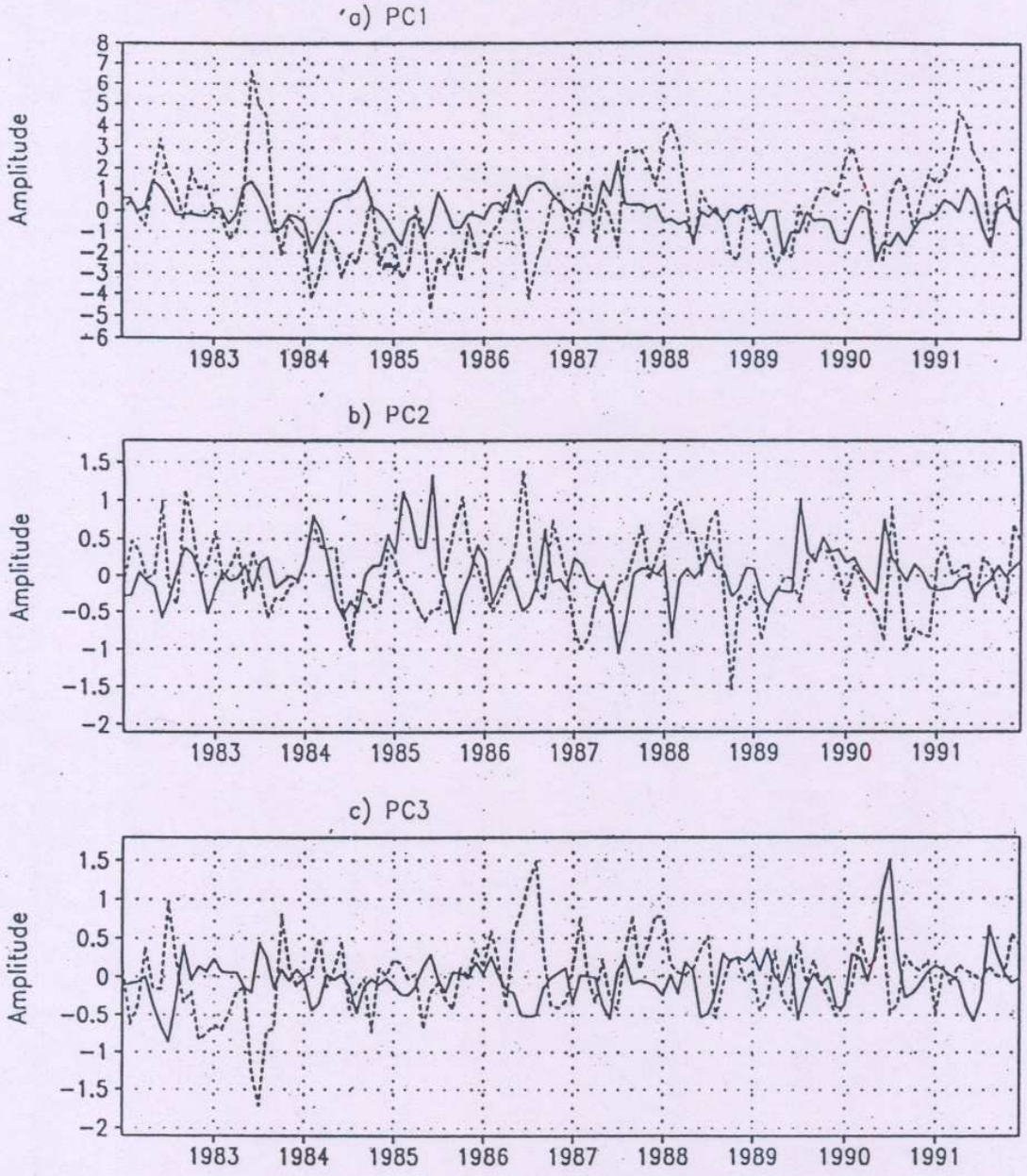

Fig. 8 Principal Components associated with first three EOFs obtained from model simulated SST anomalies (solid) and observed NCEP SST anomalies (dashed).

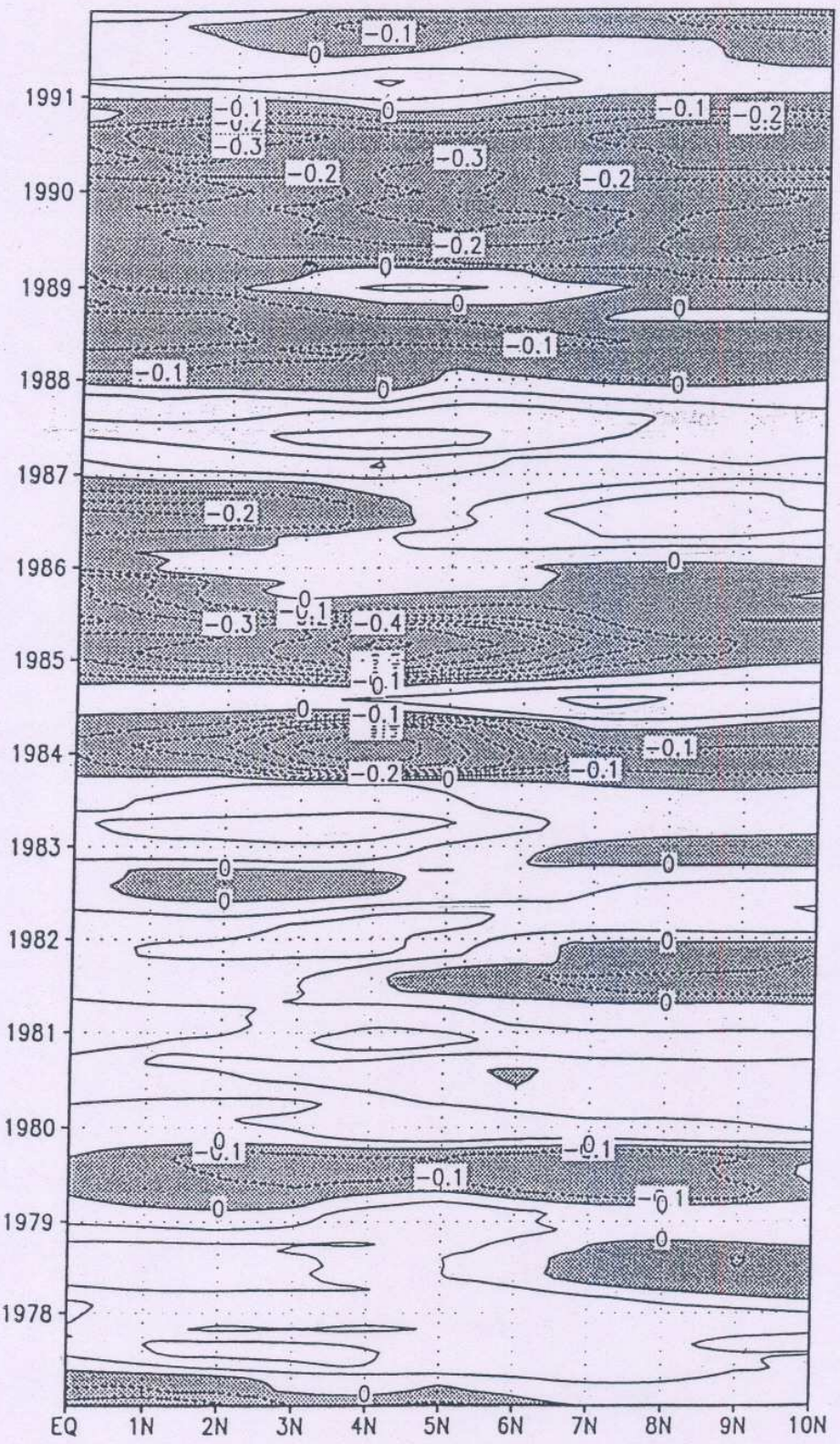

Fig. 9 Latitude –time plot of model SST anomalies along 55E for the period 1977–1991. A seven month running mean is applied on the anomalies.

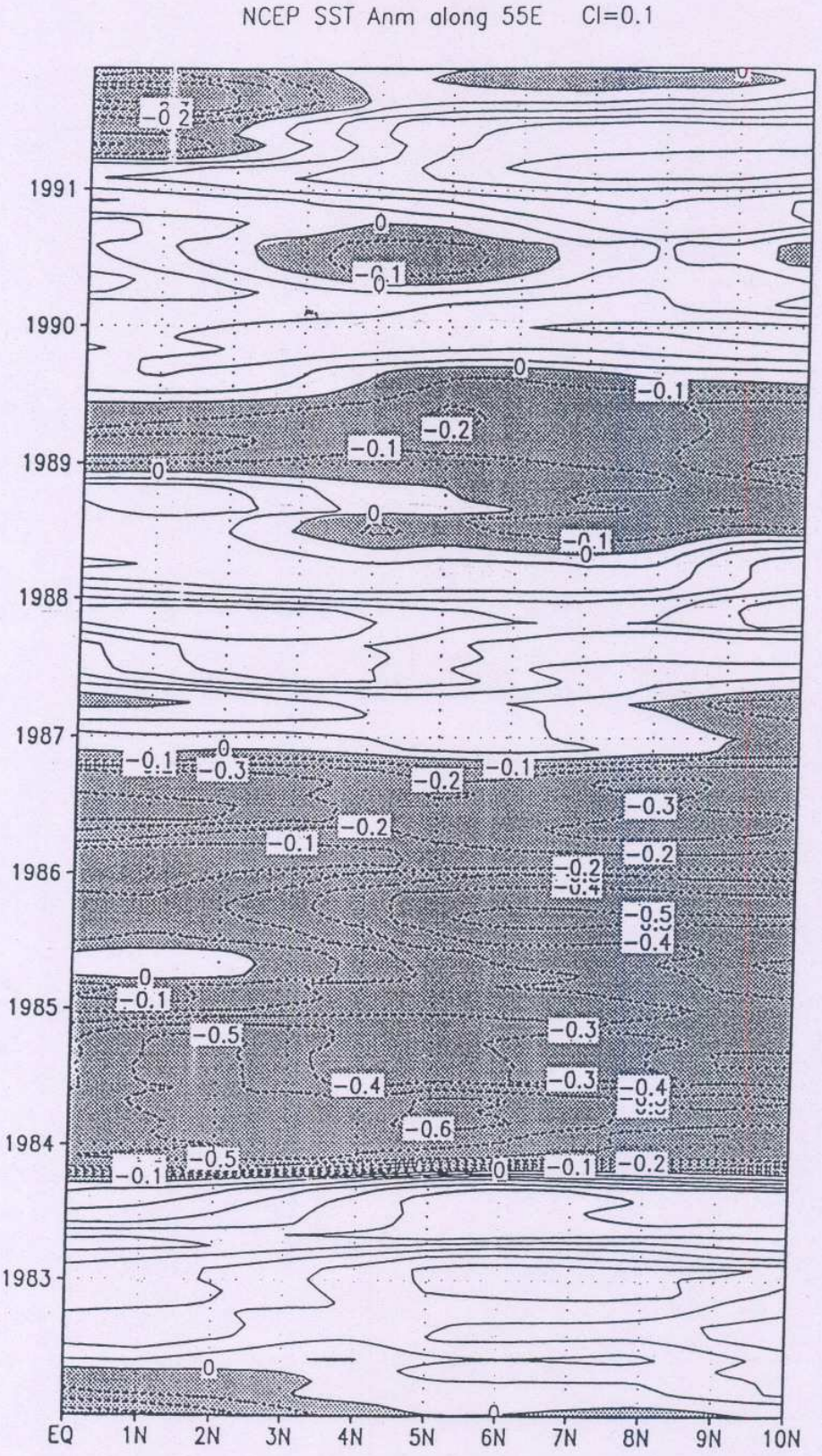

Fig. 10 Latitude–time plot of NCEP SST anomalies along 55E for the period 1982–1991. A seven month running mean is applied on the anomalies.

Figure – 11

a) Inc wind & main

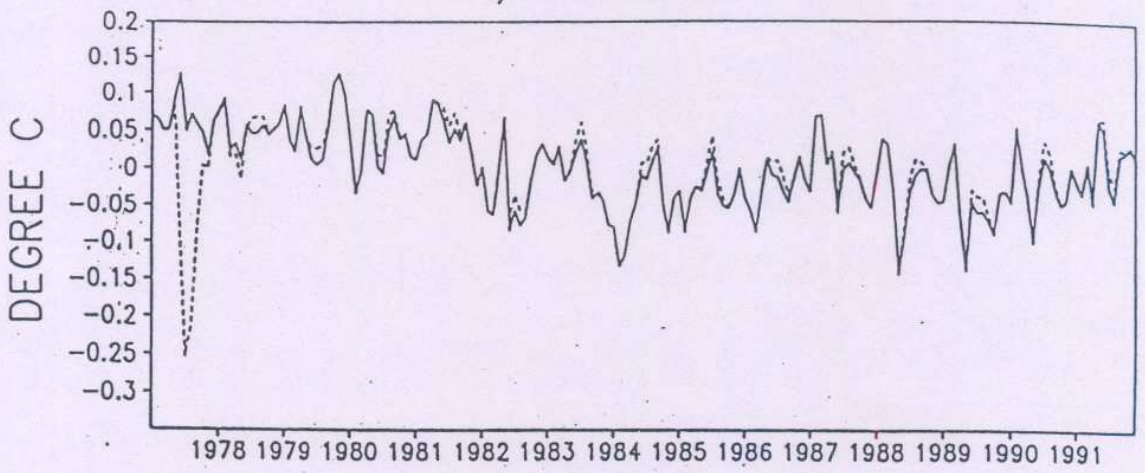

b) Dcr wind & main

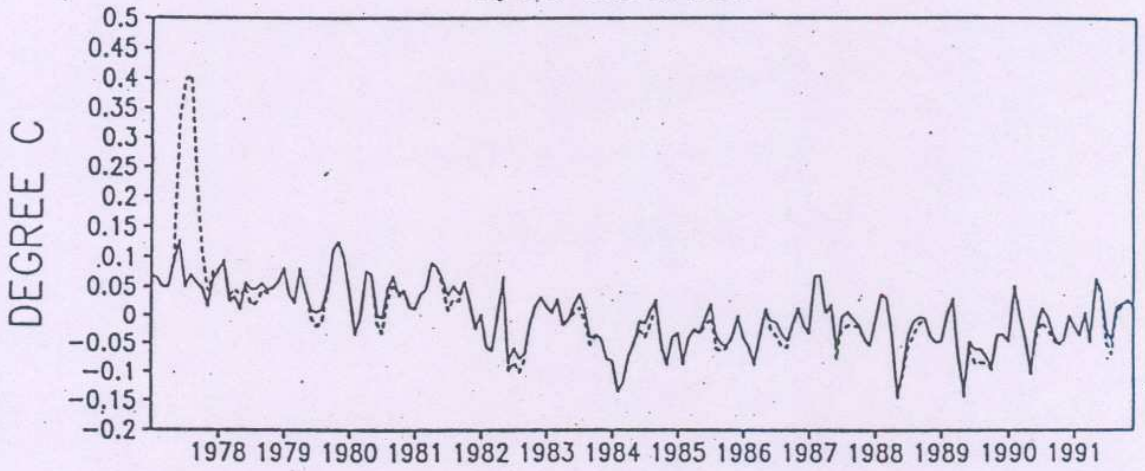

c) Incr hflux & main

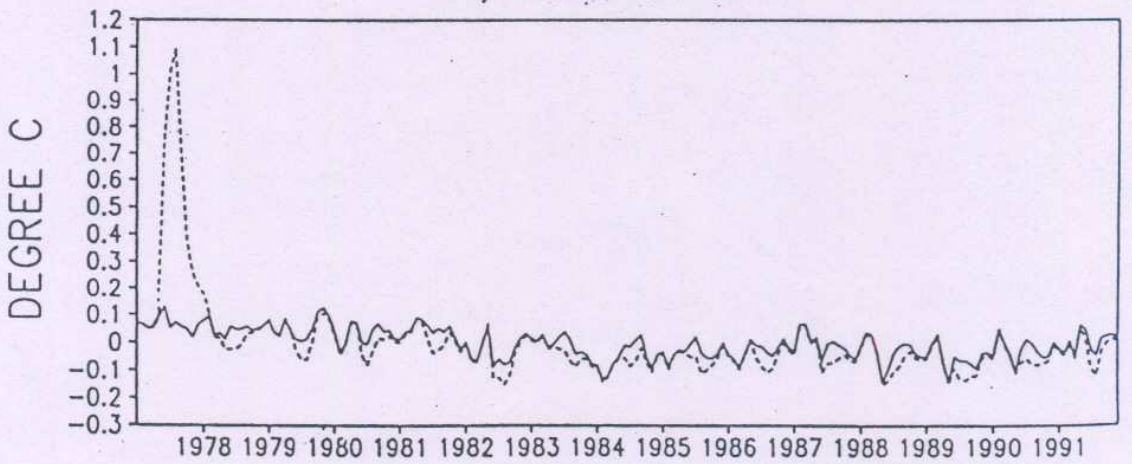

Contd....

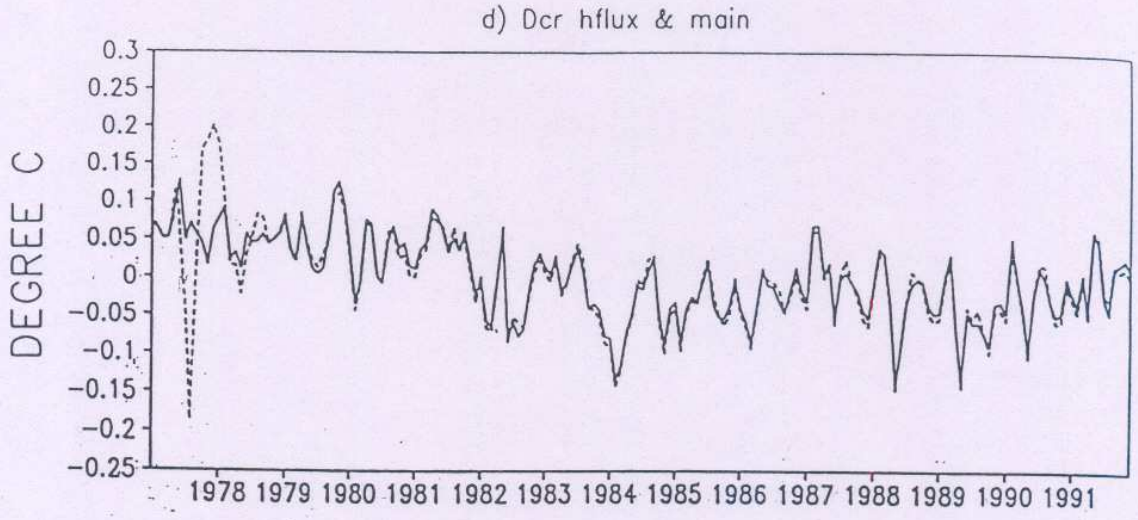

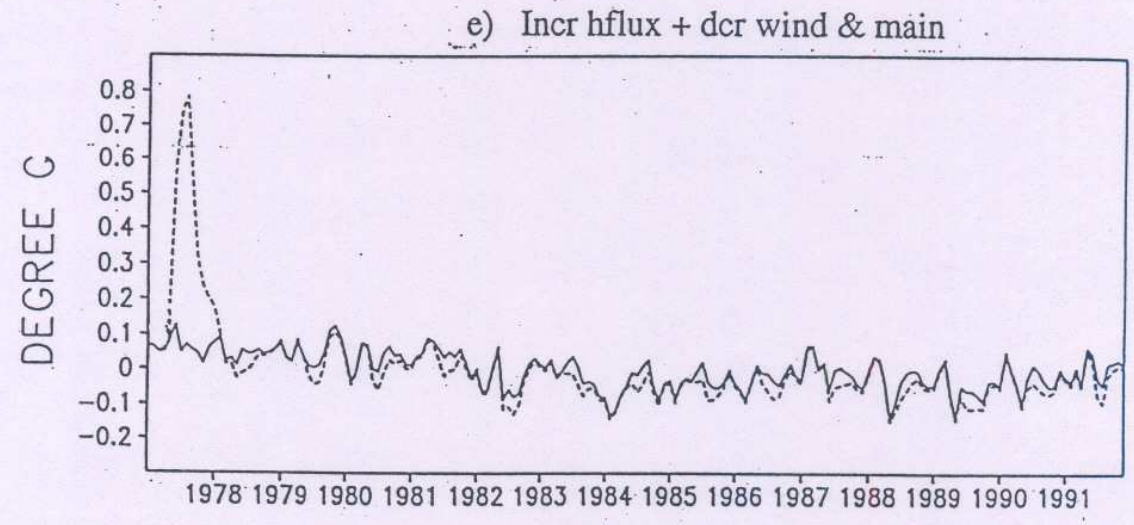

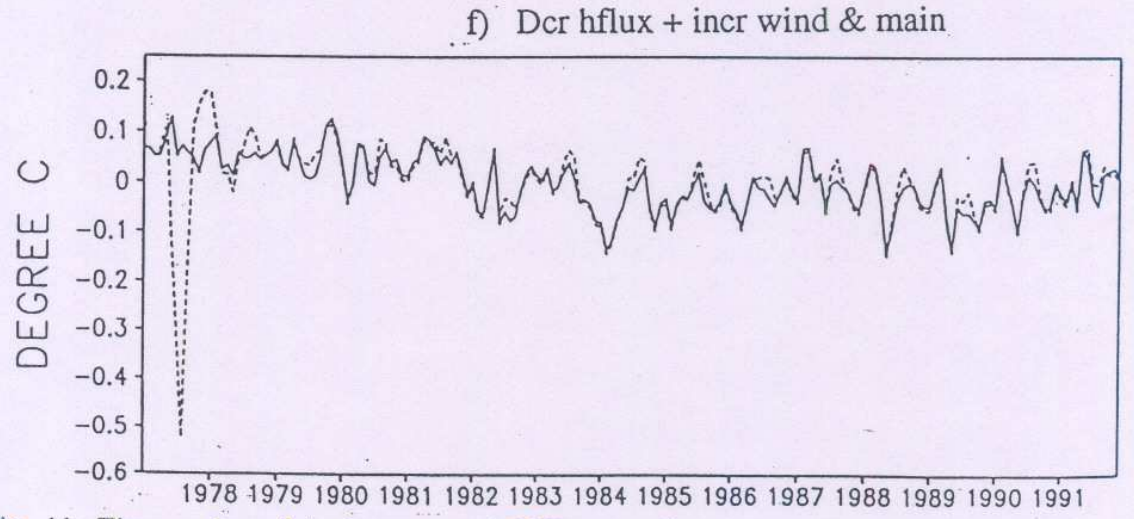

Fig. 11. Time series of basin averaged SST anomalies from the sensitivity experiments (dashed lines) , a) increased wind stress case, b) decreased wind stress case, c) increased heat flux case, d) decreased heat flux case, e) increased heat flux and decreased wind stress case & f) decreased heat flux and increased wind stress case. Superimposed is the basin averaged SST anomalies from main run.

Figure – 12

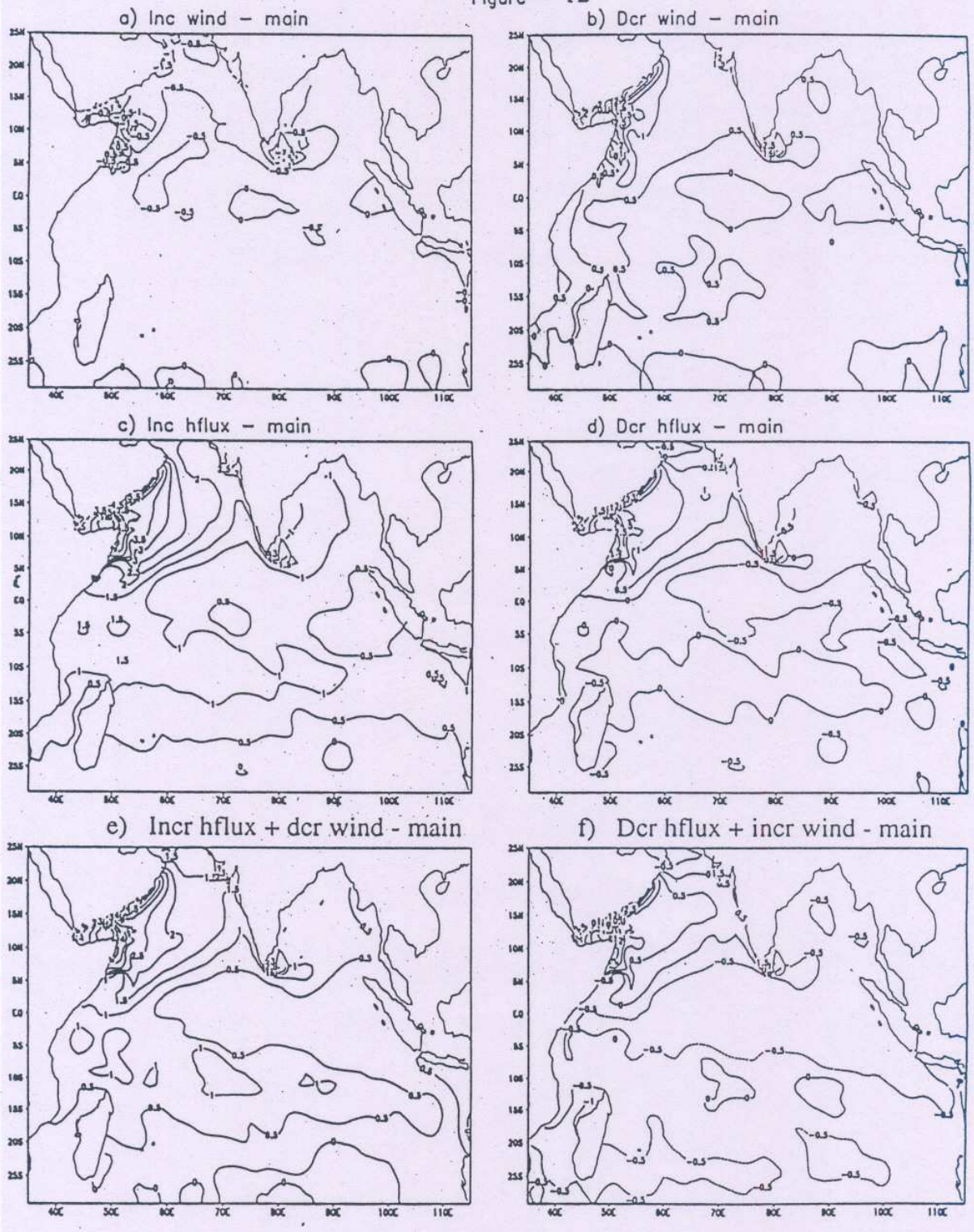

Fig. 12. The difference of SST anomalies between sensitivity experiment and main run in July, 1977: a) increased wind stress case, b) decreased wind stress case, c) increased heat flux case, d) decreased heat flux case, e) increased heat flux and decreased wind stress case & f) decreased heat flux and increased wind stress case.